

## Student Guide: Making Waves by Visualizing Fourier Transformation

**Robert Smalley, Jr.**  
Center for Earthquake Research and Information, The University of Memphis

*Online material:* Additional details of the mathematics.

### INTRODUCTION

Using a simple graphical presentation we can visualize the integrand of the forward and inverse Fourier transforms as a topographic surface. This presentation aids in understanding frequency domain and real-space relationships, such as the important, but often poorly understood, contribution of the frequency domain phase spectrum to the real-space shape. The Fourier transform integrand visualization method presented here can also help develop insights into complex wave behavior, such as the relationship between traveling and standing waves and the evolution of dispersing wavetrains.

### BACKGROUND

Fourier analysis is often introduced with a figure showing how to approximate a function by adding together sinusoids (Figure 1A). I extend this presentation through the introduction of Fourier transform integrand visualization (FTIV) and use this technique to illustrate the relationship between traveling and standing waves, the Fourier shift theorem, and how the phase affects the real-space shape of a dispersing wave.

Figure 1(A) shows a real space, in this case a time-domain function, a boxcar symmetric about  $t = 0$ , and the first few terms of its Fourier series

$$u(t) = \frac{c_0}{2} + \sum_{n=1}^{\infty} [c_n \cos(\omega_n t + \phi_n)], \quad \omega_n = n\omega_1, a_n \text{ real.} \quad (1)$$

The weights,  $c(\omega_n)$ , and phase shifts,  $(\phi_n)$ , represent  $u$  in the frequency domain. The  $\cos(\omega_n t)$  terms are known as basis functions and have variables from both domains, *i.e.*, time and frequency, in their argument. The set of basis functions must meet two important conditions. First, mutual orthogonality, which means you cannot make any of them by summing the others. Second, “completeness,” which means any arbitrary function, with some conditions to ensure convergence, can be

represented using only this set of functions. The Fourier series is also periodic, with period  $T = 2\pi/\omega_1$ .

The Fourier series can be generalized to the inverse Fourier transform

$$u(t) = \int_{-\infty}^{\infty} c(\omega) \cos(\omega t + \phi(\omega)) d\omega \quad (2)$$

where the amplitude,  $c(\omega)$ , and phase,  $\phi(\omega)$ , spectra come from the Fourier transform

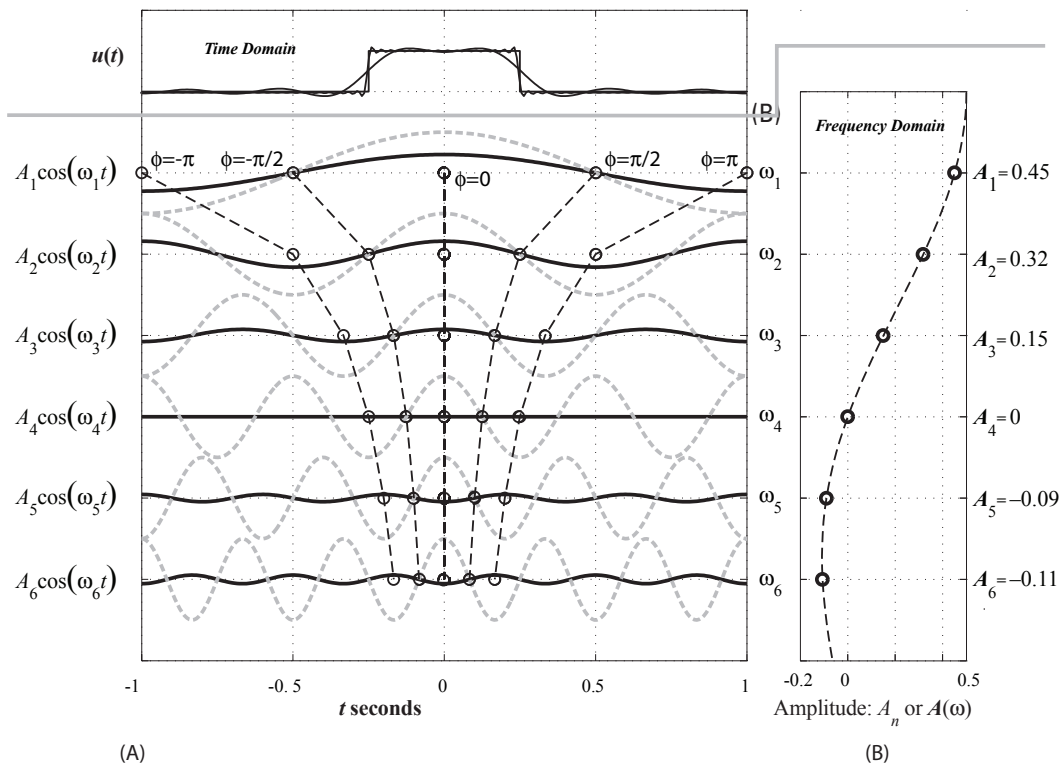
$$c(\omega) = \frac{1}{2\pi} \int_{-\infty}^{\infty} u(t) \cos(\omega t + \phi(\omega)) dt \quad (3)$$

with  $\phi(\omega)$  chosen to maximize  $|c(\omega)|$ . (The function  $u(t)$  must be absolutely integrable and non-periodic.) The amplitude and phase spectra can be interpreted through the mathematical concept of correlation, which quantifies the similarity of functions; the Fourier transform is a correlation between the time-domain function and the time-shifted basis functions. The functions  $u(t)$  and  $F(\omega) = [c(\omega), \phi(\omega)]$  are known as a Fourier transform pair.

### VISUALIZING THE FOURIER INTEGRAND

Relating frequency-domain and time-domain behaviors, especially those related to  $\phi(\omega)$ , is difficult with figures such as Figure 1(A), which typically use functions with  $\phi(\omega) = 0$ . FTIV illustrates the relationship between the Fourier transform pairs more clearly while naturally including  $\phi(\omega)$ . Figure 2(A) (shown on the back cover) introduces the FTIV technique using the basis functions of the forward and inverse Fourier transform integrands as a topographic surface. Figure 2(B) shows the inverse Fourier transform process; following the arrows, multiply the basis functions by  $c(\omega)$  to make the inverse Fourier transform integrand, then integrate to obtain the boxcar. Figure 2(C) shows the process for the Fourier transform.

The  $\phi(\omega)$  term in the basis function argument shifts the basis function's position along the real-space axis (step 0, Figure 2). This is the key to FTIV that allows showing both  $c(\omega)$  and  $\phi(\omega)$  in a clearly interpretable form. To examine the relationship between the time-domain shape and  $\phi(\omega)$ , consider a function with Fourier transform  $c(\omega) = 1$ ,  $\phi(\omega) = 0$ . This makes a time-domain delta function at  $t = 0$  (Figure 3). When  $c(\omega) = 1$ , contours of the inverse Fourier transform integrand amplitude are the same as contours of constant, or stationary, argument (we will hereafter refer to the basis function argument as the “phase”), and we will equate them. This relationship makes it



▲ **Figure 1.** (A) Time-domain boxcar approximations using 7 (heavy) and 100 (thin) Fourier series terms. First through sixth basis functions (gray dashed) and Fourier series terms (black). Points with stationary argument (circles) connected by vertical dashed lines between Fourier series terms become Fourier transform integrand lines of stationary phase. (B) Weights for Fourier series (circles) and Fourier transform (dashed line, scaled to match Fourier series).

easier to see the phase (*i.e.*, argument) behavior in Figures 2–5, which display the cosine of the phase and not the phase itself (a plot of the phase is not very illuminating).

The real-space function in Figure 3 is non-zero only at  $t = 0$ , where the phase is stationary. At  $t = 0.49$ , the phase varies linearly, and the integrand and running sum oscillate and remain small (zero). This observation is the basis of the principle of stationary phase: for functions that are oscillatory over most of their range, non-zero contributions to their integral come from integrand regions where the phase is stationary (*e.g.*, Udías 1999). We will refer to the contours seen in Figure 3 as skirts. Integrating along vertical paths, constructive/destructive interference occurs where the skirts are vertical/sloping.

## EXAMPLES

### Traveling Waves to Standing Waves and Back

Combining two sinusoidal waves traveling in opposite directions produces a standing wave (with  $k$  as “spatial frequency”)

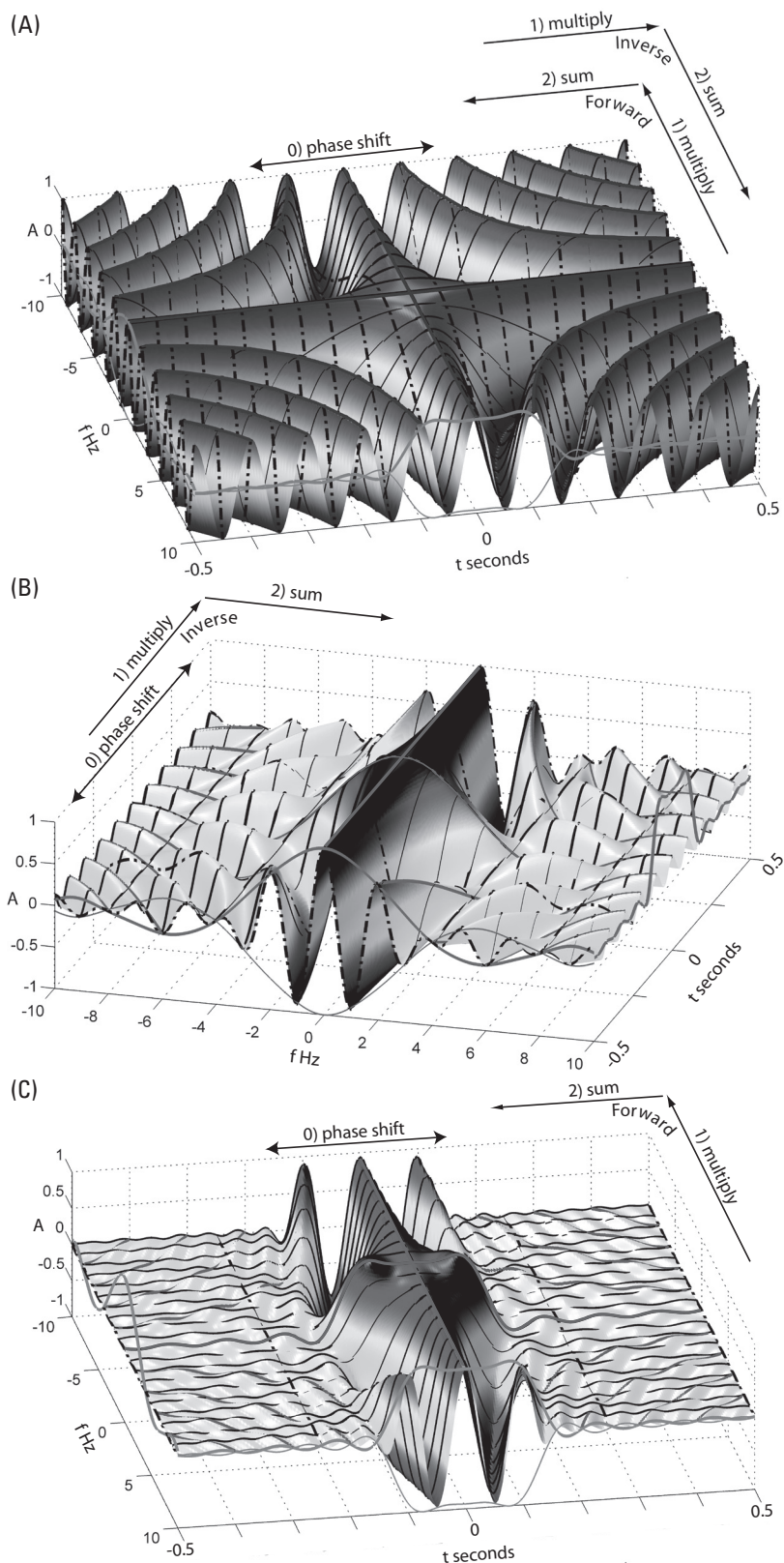
$$\begin{aligned}
 u(x, t) &= \cos(kx + \omega t) + \cos(kx - \omega t) \\
 &= 2\cos(kx)\cos(\omega t), \\
 (k &= 2\pi/\lambda, v = \omega/k). \tag{4}
 \end{aligned}$$

The right side of the equation shows a stationary wave in space,  $\cos(kx)$ , modulated in time by  $\cos(\omega t)$ . Now consider two del-

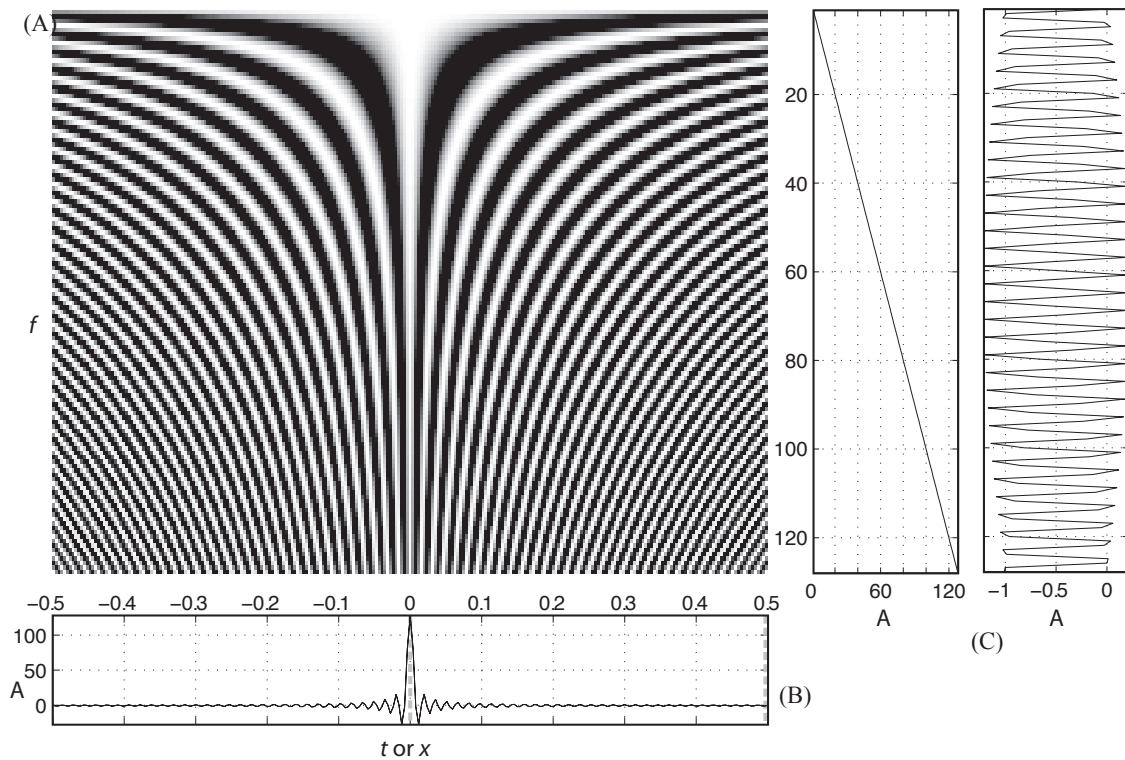
tas propagating at  $\pm v$  (Figures 4A and 4B). The inverse Fourier transform integrands of traveling sinusoidal waves and time-domain deltas move to positions  $x_1 = \pm vt_1$  at  $t_1$ . The real-space axis is now distance (distance-domain) and the real-space plot is a snapshot of the wavefield in space. Adding the wavefields of Figures 4(A)-ii and 4(B)-ii produces the wavefield in Figure 4(C)-ii. Alternately, adding the inverse Fourier transform integrands of traveling waves in Figure 4(A)-i and 4(B)-i produces an inverse Fourier transform integrand of standing waves in Figure 4(C)-i, which integrates to the traveling deltas in Figure 4(C)-ii. How do traveling waves arise from the integration of standing waves? The right side of Figure 4(C)-i shows the inverse Fourier transform integrand decomposed into the two standing wave factors, the  $\cos(kx)$  component, from  $x = 0$  to  $x = 0.1$  (the delta’s position), and the  $\cos(\omega t)$  component, from  $x = 0.1$  to  $x = 0.25$ . At  $t = t_1$ , the inverse Fourier transform is

$$u(x, t_1) = \int_{-\infty}^{\infty} \cos(\omega t_1) \cos(kx) dk \propto \delta(kx \pm \omega t_1), \tag{5}$$

giving the traveling deltas at  $x_1 = \pm \omega t_1/k = \pm vt_1$  from the orthogonality of the cosine. The  $\cos(\omega t_1)$  term selects positions of  $\cos(kx)$ , which vary with time, having the same angular frequency forming a non-oscillatory integrand  $\propto \cos^2(kx_1) = \cos^2(\omega t_1)$ . At all other positions the integrand oscillates and integrates to zero.



▲ **Figure 2.** (A) FTIV 3-D view of the common, basis function part of forward and inverse Fourier transform integrands as a surface. Frequency and time domain functions/envelopes (normalized to their maximum) shown by heavy/light plots along axes. Curves of constant amplitude and stationary phase shown on the back cover in blue. (B) Inverse Fourier transform integrand for boxcar after multiplying basis functions by  $c(\omega)$ . Sum parallel to  $f$  axis produces time-domain curve  $u(t)$  along  $t$  axis. (C) Forward Fourier transform integrand for a boxcar after multiplying basis functions by  $u(t)$ . Sum parallel to  $t$  axis produces frequency-domain curve  $C(\omega)$  along  $f$  axis.



▲ **Figure 3.** FTIV gray scale topographic view of inverse Fourier transform integrand for a delta (top) with real-space function (bottom). Plots on right show running sums of the inverse Fourier transform integrand for profiles at two times or positions (gray dashed lines).

### Fourier Shift Theorem

Shifting the delta also shifts the inverse Fourier transform integrand along the real-space axis (Figures 4A-i and 4B-i), providing a graphical view of the shift theorem: a real-space shift changes  $\phi(k) \propto (\text{real-space distance travelled}/\lambda) \propto kx$ , but does not change  $c(\omega)$ .

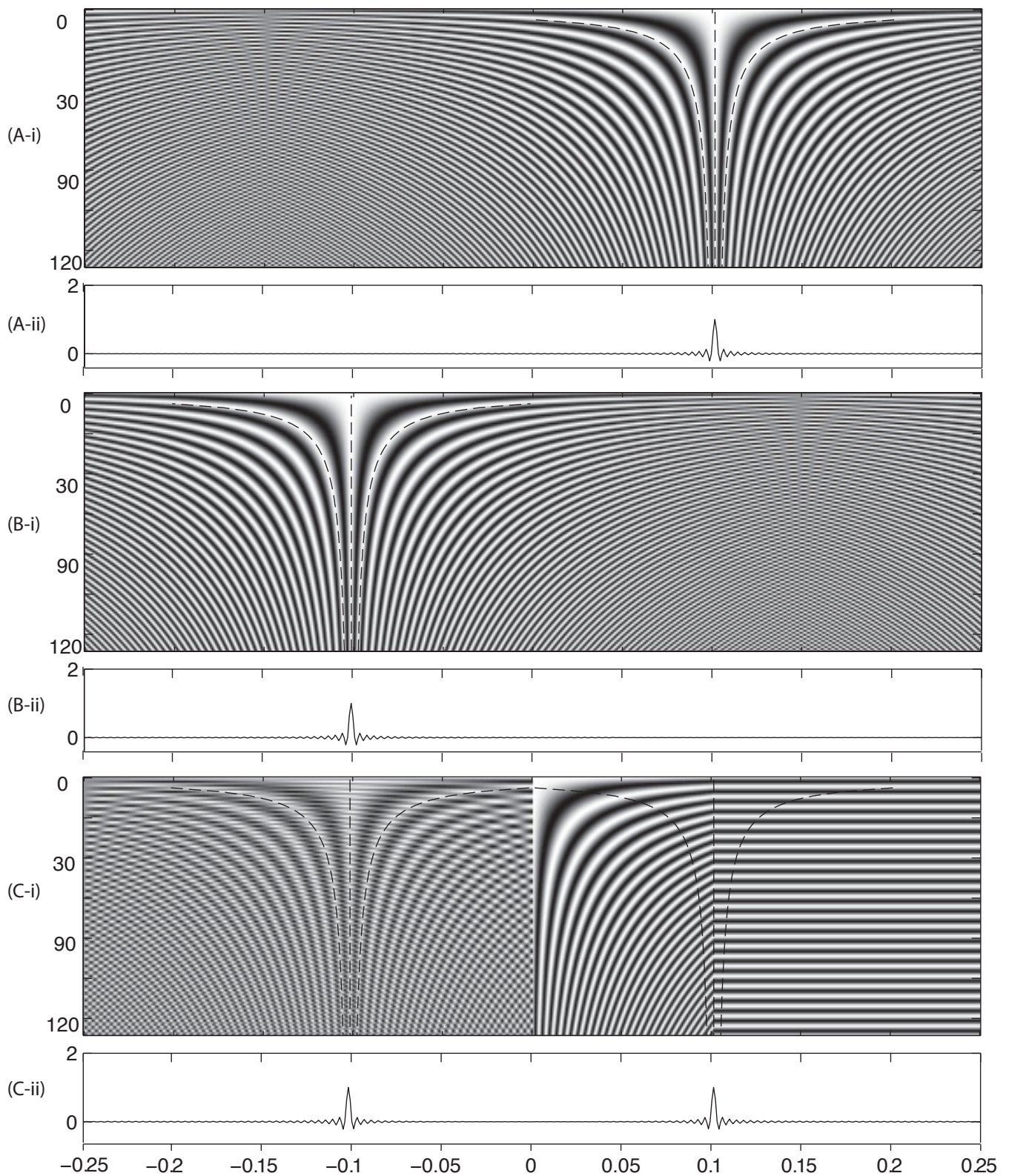
### Dispersion

When velocity is a function of frequency,  $v(k)$ , traveling waves change shape. Following Brune *et al.* (1960) and Nafe and Brune (1960), we now relate inverse Fourier transform integrand behavior to dispersion. Figure 5 (on the front cover) shows how, starting from the delta at  $t = 0$ , at  $t_1$  each inverse Fourier transform integrand component traveled  $x(k) = v(k)t_1$  to produce the inverse Fourier transform integrand (demonstrating how FTIV displays  $\phi$ ) and real-space wavefield shown. The vertical line of stationary phase at  $x = 0, t = 0$  is sheared into a new shape (Figure 5A, see cyan line on front cover) and initially sloping inverse Fourier transform integrand skirts fold and go through vertical. The wavefield also evolved into a wide, complex shape in the region  $v_3t_1 < x < v_1t_1$ , which is wider than expected from the fast and slow velocity limits,  $v_2t_1 < x < v_1t_1$ . Where does the low velocity limit,  $v_3$ , come from? The answer is found by analyzing the skirt pattern.

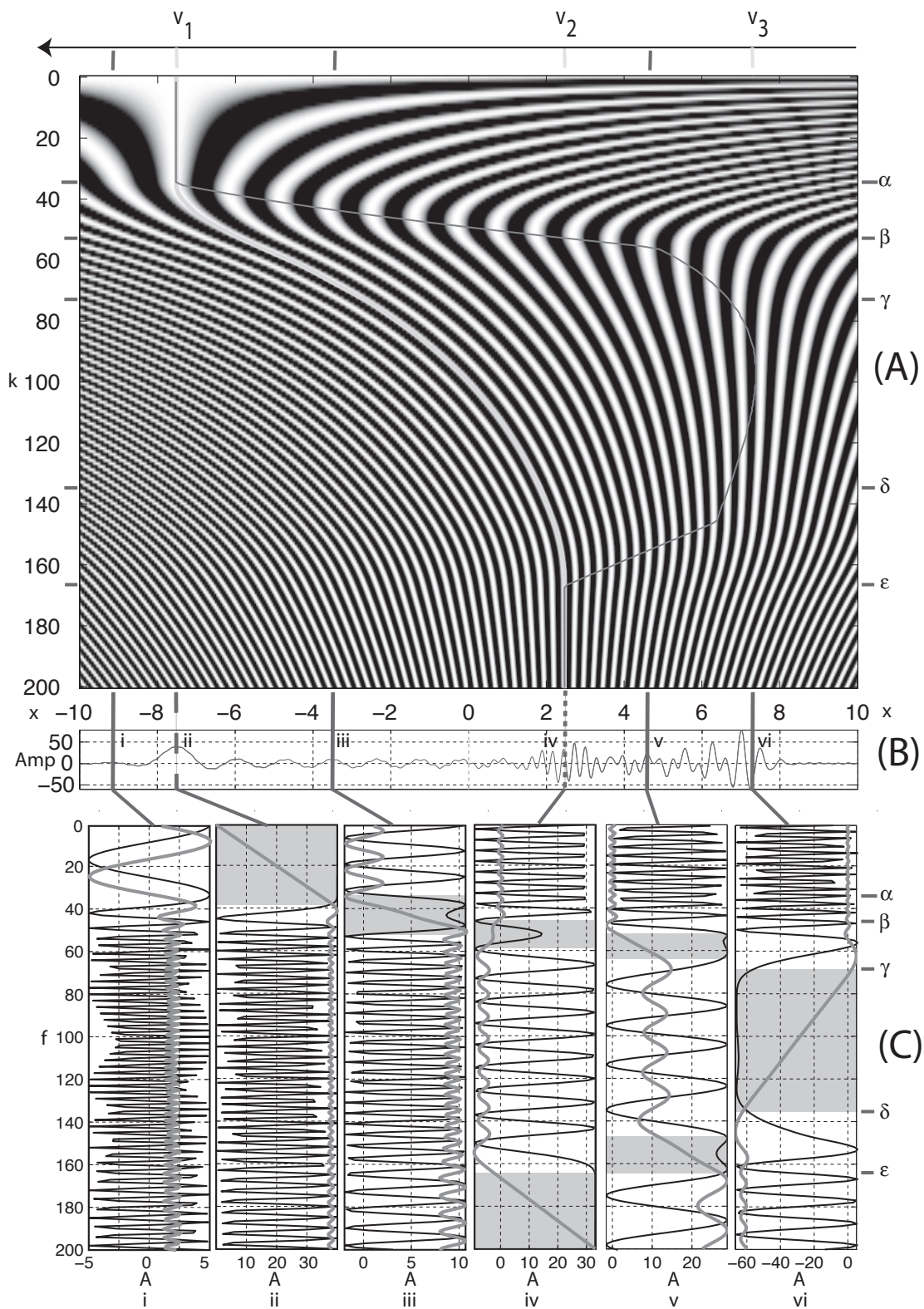
Left of  $v_1$  and right of  $v_3$  the skirts slope, the integral is zero (Figure 5C-i, vi), and the real-space wave is not found. At  $v_1$ , the skirt is vertical for  $0 < k < \alpha$ , then slopes for  $\alpha < k$ . As regions with sloping skirts do not contribute to the integral, we can integrate over only  $0 < k < \alpha$  to obtain  $u(x, t) \propto$

$\text{sinc}(X) \cos(k_0x - \omega_0t)$ ,  $X \propto (x - v_1t)\delta k$ , (Udías 1999). This is the product of a traveling sinusoidal carrier,  $\cos(k_0x - \omega_0t)$ , and a sinc modulation. The  $(x - v_1t)$  term shifts the sinc's location by  $v_1t$ , while  $\delta k$  controls its width. A similar analysis can be done at  $v_2$  for  $\delta < k$ . If the sinc is narrower than the sinusoids' wavelength the result looks like a sinc pulse ( $x \approx -7.5$ , Figure 5B-ii). If it is wider, the result looks like a sinusoidal wave with a sinc envelope ( $x \approx 3.5$ , Figure 5B-iv). The sinc envelopes move at  $v_1$  or  $v_2$  respectively, and restrict the wavefield to finite regions containing the wave's energy. The real-space wavefield comes from regions where the integrand's phase is stationary (Figure 5 C-ii and iv, gray background).

Between  $v_1$  and  $v_2$  the skirts fold. Here, waves with an observed  $k$  in the real-space wavefield, found by integrating the inverse Fourier transform integrand, do not travel at the  $v(k)$  shown by the cyan curve. They are found to travel at a velocity defined by the magenta curve (Figure 5A). The magenta curve connects the set of points in the inverse Fourier transform integrand having stationary phase (vertical skirts) and defines a new type of velocity, the group velocity,  $v_g(k)$ , at which waves (and energy, etc.) travel in the real-space. The  $k$  and  $v$  observed at position  $x$  of the real-space wave (Figure 5B) are the same as those associated with the point of stationary phase,  $(x, k)$ , on the magenta curve in the inverse Fourier transform integrand (Figure 5A). Figure 5 illustrates that phase velocity is easy to understand but hard to measure (nothing is physically traveling at the phase velocity), and that group velocity is hard to understand but easy to measure (it is the velocity of the physical wavefield we observe).



▲ **Figure 4.** Traveling waves in FTIV view of (A-i) and (B-i) combine into standing waves in the left side of (C-i). Solid and dashed curves in (A-i) and (B-i) show lines of stationary phase. These lines are also drawn in (C-i), where one sees a resemblance of the skirt patterns. Right side of (C-i) shows product form: a fixed spatial delta,  $\cos(kx)$ , modulated by  $\cos(\omega x)$ . Real-space traveling deltas from integration if inverse Fourier transform integrands are shown in (A-ii), (B-ii) and (C-ii).



▲ **Figure 5.** Illustration of dispersion, phase and group velocities, and principle of stationary phase. (A) Inverse Fourier transform integrand ( $\cos(kx - \omega(k)t)$ ,  $v(k) = \omega(k)/k$ ) and (B) plot of dispersed wave. The distance axis, shared by inverse Fourier transform integrand and real-space plots, pans with the wave. Rescaling the  $x$  axis by  $1/t_1$  changes it to velocity (top) with phase and group velocities shown by cyan and magenta curves on the front cover. Yellow ticks on  $v$  axis mark fast and slow limits of phase and group velocities. (C) Inverse Fourier transform integrand profiles (black, scale  $\pm 1$ ) and running sums (red, i through vi, scale labeled). Ticks on  $k$  axis (A and C, right side) mark frequency bands for classes of real-space behavior associated with regions of stationary phase (gray background).

The inverse Fourier transform integrand skirt pattern, real-space shape, and group velocity are related by the principle of stationary phase, which applies to integrating the product of a slowly varying function and a rapidly oscillating function (see Båth 1968). In our case, the slowly varying function is  $c(k) = 1$ , and we only have to consider the oscillatory term,  $\cos(kx - \omega(k)t)$ , greatly simplifying the discussion without losing insight. When the phase is stationary (constant, vertical skirt),

$$\begin{aligned} (kx - \omega(k)t) &= Y(k, x) = C, \\ \partial Y / \partial k|_x &= 0, \\ x/t = d\omega(k)/dk|_x &= U(k). \end{aligned} \quad (6)$$

The contribution to the wavefield from Fourier component  $k$  arrives at  $x$  at velocity  $v_g = U(k)$ . A branch of stationary phase is found between  $v_2 t_1 < x < v_1 t_1$  in  $\alpha < k < \beta$ , producing a sinusoidal wavefield of slowly decreasing wavelength. A running sum (Figure 5C-iii) shows that the largest contribution to the wavefield comes from the small region  $(x, k)$  (gray background) of the skirt pattern fold where the phase is stationary. There are two stationary phase branches in  $v_3 t_1 < x < v_2 t_1$ ,  $\beta < k < \gamma$  and  $\delta < k < \varepsilon$ , and the non-zero contributions come from the two stationary phase regions (Figure 5C-v).

Finally,  $v_3$  is an inflection point where the second derivative of the phase is also zero, indicated by the vertical skirt in  $\gamma < k < \delta$  that does not form a closed fold. Using an extension of the principle of stationary phase, we obtain a large amplitude pulse known as the Airy phase, associated with an extremum (minimum) of the group velocity (Figure 5C-vi).

## DISCUSSION AND CONCLUSIONS

We have seen that  $\phi(\omega)$  can have significant effects on the real-space shape. How does this compare to the effects of  $c(\omega)$ ? The

shape of the boxcar comes from  $c(\omega)$ . We saw that a delta with  $c(\omega) = 1$  and  $\phi(\omega) = 0$  can generate a dispersed seismogram through variation of only the phase spectrum. For  $c(\omega) = 1$  and random phase, the time-domain function is white noise. The delta, white noise, and dispersed wavetrain all have  $c(\omega) = 1$ , but different real-space functions determined by  $\phi(\omega)$ , which shows that the phase spectrum carries important information and can be a major contributor to the real-space shape and its time evolution. The shape of a wave as it propagates depends on changes in both  $c(\omega)$  and  $\phi(\omega)$ . Viewing the forward and inverse Fourier transform integrands as a topographic surface provides insight into a number of real-space wavefield features such as the often underappreciated phase spectrum contribution to the real-space function, how to make traveling waves from standing waves, and the behavior of dispersing wavefields. 

## ACKNOWLEDGMENTS

I thank C. Langston, J. Pujol, M. Bevis, and *SRL* Editor L. Astiz for helpful reviews.

## REFERENCES

- Båth, M. (1968). *Mathematical Aspects of Seismology*. Developments in Solid Earth Geophysics 4. New York: Elsevier, 415 pps.
- Brune, J. N., J. E. Nafe, and J. E. Oliver (1960). A simplified method for the analysis and synthesis of dispersed wave trains. *Journal of Geophysical Research* **65** (1), 287–304.
- Nafe, J. E., and J. N. Brune (1960). Observations of phase velocity for Rayleigh waves in the period range 100 to 400 seconds. *Bulletin of the Seismological Society of America* **50** (3), 427–439.
- Udías, A. (1999). *Principles of Seismology*. Cambridge: Cambridge Univ. Press, 475 pps.

*Center for Earthquake Research and Information*  
*University of Memphis*  
*Memphis, Tennessee 38152 U.S.A.*  
*smalley@ceri.memphis.edu*